

Single-motor Ultraflexible Robotic (SMUFR) Humanoid Hand

Quan Xiong, Dannuo Li, Xuanyi Zhou, Wenci Xin, Chao Wang, Jonathan William Ambrose and Raye Chen-Hua Yeow, *Member, IEEE*

Abstract— Humanoid robotic hands have significant potential in easing human burden and augmenting human labour. This paper introduces the SMUFR hand, a compliant and dexterous robotic humanoid hand powered by tendon-driven mechanisms, and features flexible beam-based bending joints serving as rotary joints with bidirectional bending compliance that ensure safety during human-robot interaction. Despite its light weight of only 363 g without remote transmission and actuation components, the SMUFR hand can grasp and support loads of up to 4.2 kg in various orientations, manipulate objects of different sizes and shapes, and even operate underwater. Of particular note is the SMUFR hand's lightweight and compact one-to-more actuation system, comprising six rotary pneumatic clutches (RPC) for six active Degrees of Freedom (DoFs), all powered by a single motor. Each RPC, weighing 75 g, can exert up to 23 N force on the tendon. This innovative transmission system distributes the power of a single motor across five fingers and holds potential for configuring additional RPCs. We also integrated all the components on a compact wearable vest for potential mobile humanoid robotic applications. Additionally, a mathematical model was developed to predict tendon force and joint bending using the constant curvature deformation hypothesis. Experimental validation demonstrates the durability of both the RPC and the beam-based fingers of the SMUFR hand, which are capable of enduring up to 22,000 and 30,000 cycles, respectively.

Index Terms—Humanoid robotics, robotic hand, beam-based compliant joint, on-to-more transmission, rotary pneumatic clutch, human-robot interaction, grasping, soft robotics.

I. INTRODUCTION

HUMANOID robots, characterized by their human-like appearance and capabilities, are revolutionizing various industries with their potential to collaborate seamlessly with humans[1], [2]. They can perform tasks ranging from assisting in household chores to augmenting

This work was supported by National Robotics Programme–Robotics Enabling Capabilities and Technologies (W2025d0243). (Quan Xiong and Dannuo Li contributed equally to this work.) (*Corresponding author: Quan Xiong; Raye Chen-Hua Yeow*).

Quan Xiong, Dannuo Li, Xuanyi Zhou, Jonathan William Ambrose and Raye Chen-Hua Yeow are with the Evolution Innovation Lab, Department of Biomedical Engineering, National University of Singapore, Singapore, 117583 Singapore (e-mail: e0788090@u.nus.edu; ldannuo@gmail.com; zhou447837285@gmail.com; jwa@u.nus.edu; rayeyeow@nus.edu.sg).

Quan Xiong, Wenci Xin and Chao Wang are with the Advanced Robotics Centre, National University of Singapore, Singapore, 117608 Singapore (e-mail: e0788090@u.nus.edu; wxin@u.nus.edu; wangchao9203@163.com).

Raye Chen-Hua Yeow is also with Computer Science & Artificial Intelligence Laboratory, Massachusetts Institute of Technology, 02139, United States (rayeyeow@mit.edu).

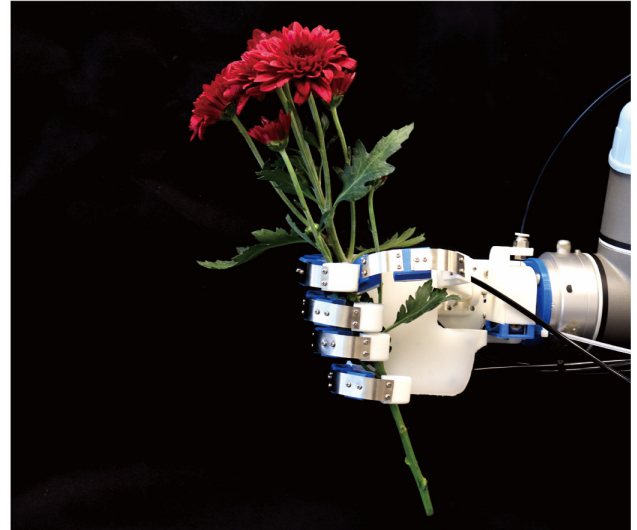


Fig. 1. The SMUFR hand holding flowers.

workforce productivity in industrial settings[3], [4]. Humanoid robotic hands, in particular, play a crucial role in replicating human activities and interacting with humans and the external environment [5], [6]. Over the past few years, humanoid robotic hands have been developed [7]–[9] to mimic the biomechanics of the human finger with joints such as distal interphalangeal (DIP), proximal interphalangeal (PIP), and metacarpophalangeal (MCP) joints, which configure one actuated degree of freedom (DoF) per finger, making them underactuated. However, traditional robotic hands often integrate rigid joints and links alongside high reduction ratio transmission systems [10]–[12], resulting in low backdrivability. This characteristic makes them vulnerable to damage during interactions with the environment. Furthermore, the high stiffness of the robotic hands increases the risk of human injury in the event of accidental collision.

To address these problems, researchers have presented compliant robotic humanoid hands using fully soft links, joints, and actuation. These soft robotic hands are generally made from soft materials such as silicone, and driven by pneumatic pressure [13]–[16], making them highly compliant and inherently safe. However, they struggle to provide the necessary grasping force and holding force when manipulating heavy items. Another approach is to combine rigid links with compliant joints using elastic components like springs, which act as buffers and restore to the initial position. Researchers have also adopted a tendon-driven method [17]–[19] to actuate

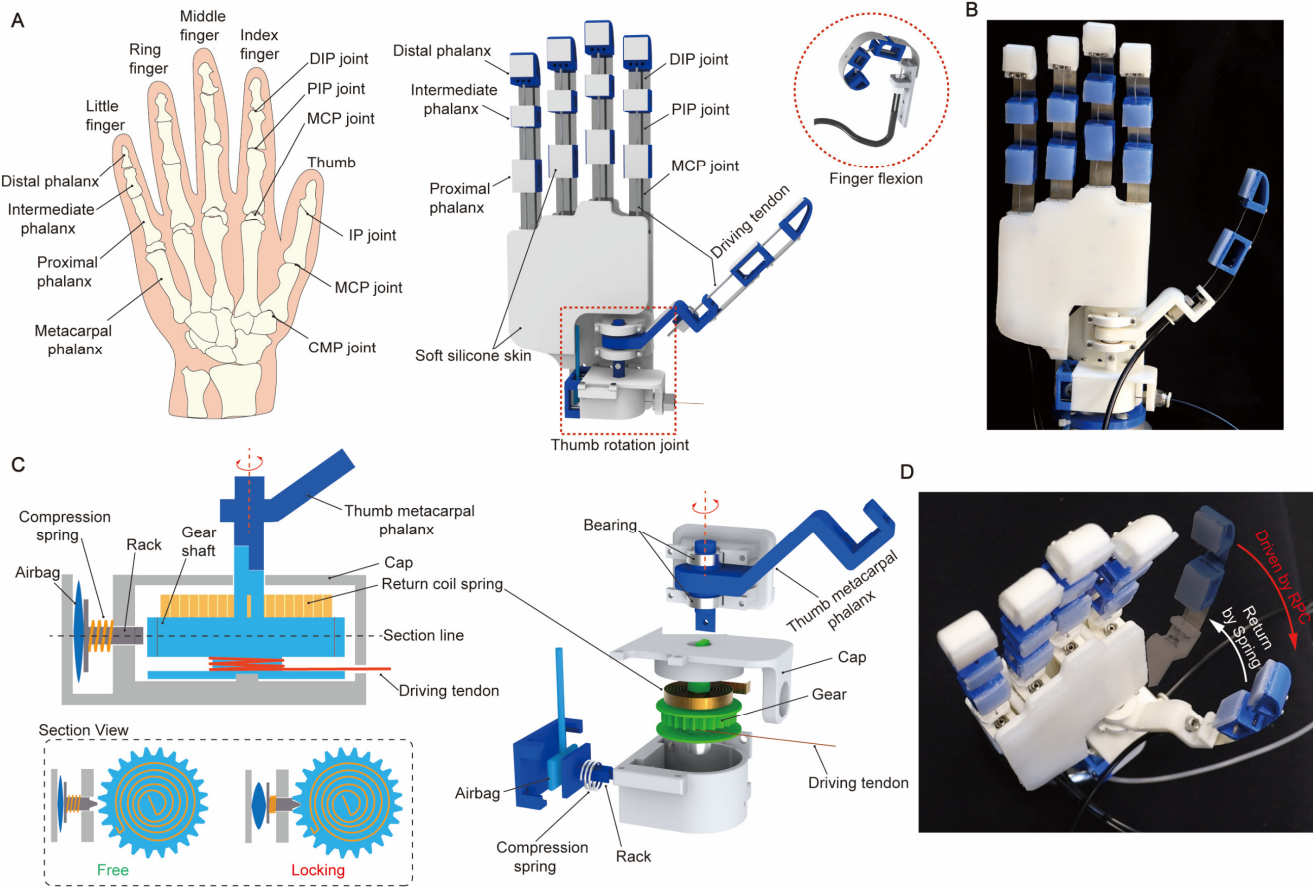


Fig. 2. Design of the robotic humanoid hand. (A) The anatomic structure of human hand and the DoF configuration of SMUFR hand in CAD. The finger flexes its joints by pulling the tendon. (B) The actual assembled SMUFR hand. (C) The design of the thumb rotation joint with pneumatic locking mechanism. (D) The thumb can rotate to a target position and stay, and then return to its initial position.

robotic fingers, which provides sufficient force to manipulate heavy loads and reduce the weight of the robotic hand. However, conventional spring-based compliant joints typically require a one-way motion-limit structure to resist the pre-stretch of springs, limiting the joint to one-way compliance [20]–[23].

Designing robotic humanoid hands to mimic real human hands necessitates incorporating numerous Degrees of Freedom (DoFs), which requires many actuators or motors. However, this presents a significant challenge in achieving a lightweight and compact actuation system. The one-to-more transmission which requires a single motor but actuates more DoFs has been applied as a promising method to resolve this problem in some wearable robotic systems[24], [25]. However, they usually use electromagnetic or magnetorheological clutches which are expensive. Moreover, active electromagnetic clutches exhibit a comparatively low torque density and significant mass [26]. While active magnetorheological clutches are heavy and require high continuous power for sustained activity, they have the capability to generate substantial torques [27], [28]. On the other hand, passive locking clutches often involve compromises in terms of kinematics and controllability,

necessitating customized designs tailored to specific applications [29]. These clutches also lack the ability to swiftly and automatically adjust stiffness. Due to the limitation of such clutches, the actuated DoFs of conventional one-to-more transmissions are restricted to less than 3.

In this work, we proposed an ultra-flexible robotic humanoid hand driven by a single motor (SMUFR hand, Fig. 1). The finger flexion joints in our robotic humanoid hand are made of flexible metal beams (stainless steel sheet), which are elastic and compliant. A tendon pulling the link connected to the flexible metal beam causes the beam to bend like a rotary joint. To achieve dexterity and decrease the weight of the actuation system, we adopted one-to-more transmission for our robotic hands. Six rotary pneumatic clutches (RPC) are connected in parallel and driven by a single motor. These clutches are independently controlled and can output power to six tendons, respectively corresponding to the flexion of five fingers and the rotation of the thumb (6 DoFs). The RPCs used in the SMUFR hand utilize fabric pneumatic actuators, which allow them to be light weight, low cost and easy to fabricate. Furthermore, the output stiffness of the RPCs (related to the maximum output force) can be regulated simply by regulating the air pressure of the fabric pneumatic actuators. A

mathematical model was developed to describe the relationship between the maximum output force of each RPC with the input pneumatic pressure. Furthermore, another simplified mathematical model was also developed to predict the tendon force and the bending angles of the joints based on the constant curvature hypothesis. Through experiments, we verified the dexterity and grasping functionality of the SMUFR hand. Additionally, the experimental results also indicated its environment adaptability, high load capability and safety of interaction with a human.

The main contributions of this article are as follows. Firstly, we present a beam-based compliant joint for a robotic humanoid hand. The joint possesses bidirectional compliance without any motion-limit structures, compared with previous spring-based compliant joints. Secondly, we designed a compact tendon-driven rotary joint with a pneumatic locking mechanism for thumb rotation that can precisely adjust the position of the thumb for improved grasping performance. Thirdly, we propose paralleled rotary pneumatic clutches to split the power from a single motor to every finger. Last, we built a practical mathematic model to predict the tendon force and bending of the joint, enabling future potential designers to use it as a reference.

II. DESIGN AND PROTOTYPE

A. Robotic Humanoid Hand

From the anatomic structure of the human hand (see Fig. 2A), all fingers except the thumb are similar and have three joints (DIP, PIP, and MCP joints) and four phalanxes (distal, intermediate, proximal, and metacarpal phalanxes). As for the thumb, it has only three phalanxes and three joints (interphalangeal, metacarpophalangeal, and carpometacarpal joints). Among all these joints, DIP, PIP, IP, and thumb MCP joints have one DoF. MCP joints of the other four fingers and the CMP joint have two DOFs. Similar to the mainstream DoF configuration of other robotic hands [20], [30]–[32] we applied two actuated tendon-driven DoFs for thumb flexion and rotation of our SMUFR hand, and one DoF for flexion of the other fingers. These underactuated fingers can adapt their shape to envelope objects well. The compliant joint in our robotic hand consists of a tendon, a flexible metal beam, and phalanxes (see Fig. 2A and B). A thin metal sheet made of 301 stainless steel is connected with two 3D-printed polylactide (PLA) phalanxes. For finger flexion, we design a through-hole for each phalanx. One side of the tendon is fixed with the distal phalanx and the tendon passes through all phalanxes of the finger via holes on phalanxes. When pulling the tendon of a finger, all the metal beams of this finger will bend simultaneously, like rotary joints (see Fig. 2A). Bowden tubes known for its low weight to high power ration are selected to transmit remote power to the robotic hand. The SMUFR hand without transmission and actuation has a low weight of a mere 363 g, which can help to reduce user fatigue.

B. Thumb Rotation Joint

The rotation of the thumb enables the robotic hand to

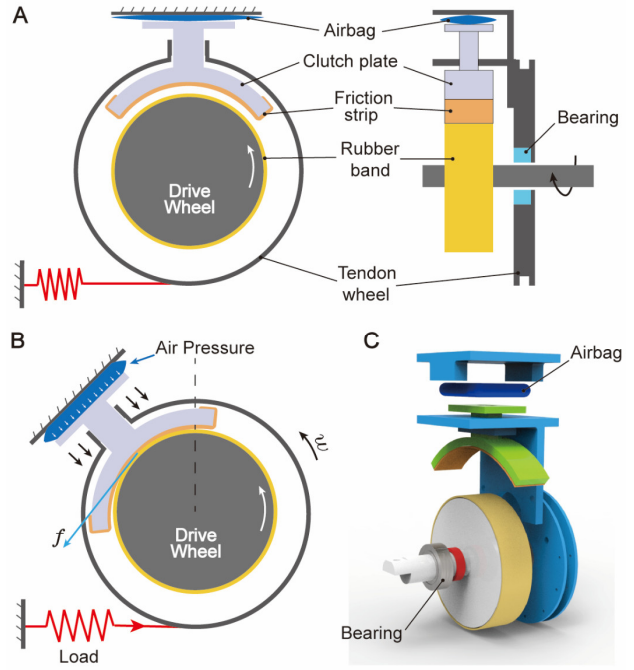


Fig. 3. Design of the RPC. (A) The structure of the RPC. (B) The activated RPC transmits force to actuate a load. (C) The assembling of the RPC.

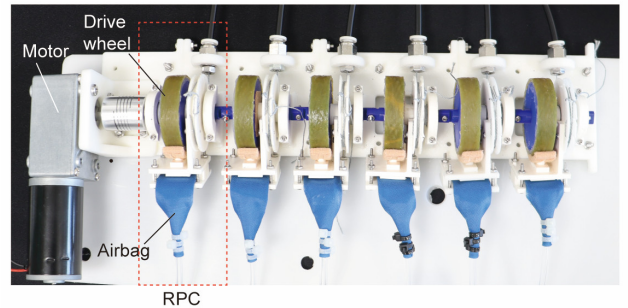


Fig. 4. The one-to-more transmission.

adaptively grasp objects of different sizes and shapes. Considering the overturning moment applied on the thumb metacarpal phalanx, we first fixed the MCP phalanx with two force-enclosed bearings (see Fig. 2A and C) that restrict the MCP phalanx to rotation motion only. We then designed a tendon-driven rotary joint (see Fig. 2C) to output a rotary moment to the MCP phalanx. The tendon was wound around a gear shaft which was connected to the MCP phalanx. Pulling the tendon turns the gear shaft and the MCP phalanx clockwise (see Fig. 2D and Video S1). A return coil spring was used to turn the MCP phalanx back to its initial position, since the restoring moment of the coil spring is counterclockwise. The inner side of the coil spring is fixed on the gear shaft and the outer side is fixed on the cap.

In addition, a locking mechanism is also needed to decouple the thumb rotation and finger flexion. For the whole grasping procedure, the thumb first rotates to the desired position, followed by the flexion of the fingers. Thus, we designed a

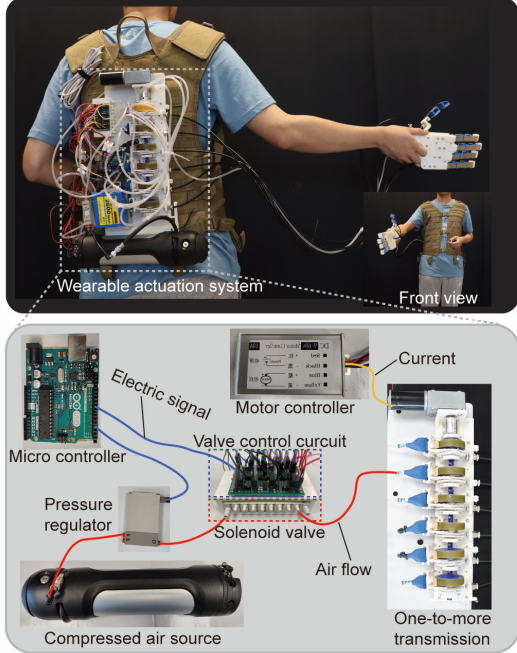


Fig. 5. Portable circuit system and the hardware design.

locking mechanism to hold the thumb MCP position (see Fig. 2C). We adopted a rack to stick the gear shaft and lock the MCP phalanx. The rack is pushed by a fabric airbag with pneumatic pressure. A compression spring is applied to provide enough resilience force to push the rack back and release the gear shaft (see Video S1).

C. Rotary Pneumatic Clutch

The clutch design is significant for one-to-more transmission. The principle of our clutches (RPC) involves using pneumatic pressure to generate friction and split the power to the tendons. As shown in Fig.3A and C, a drive wheel is connected to a DC geared motor (WS-4058GW-31ZY, Weisheng motor, 450 g weight) by a shaft allowing the drive wheel to rotate with the DC motor, and a tendon wheel is also mounted on the same shaft through a bearing. A clutch plate and its housing are mounted on the edge of the tendon wheel. The clutch plate is actuated by an airbag which is made by heat-sealing two TPU-based fabrics. We stick a friction strip on the surface of the clutch plate and a rubber band to increase friction. If no pneumatic pressure is applied to the airbag, the friction between the drive wheel and the clutch plate is very low and the tendon wheel cannot rotate with the drive wheel. However, applying pneumatic pressure will cause the friction strip on the clutch plate to press against the rubber band on the drive wheel, increasing the friction between the clutch plate and the drive wheel. This results in clutching of the tendon wheel, causing it to rotate synchronously with the drive wheel, which also pulls the attached tendon and thus applying load (see Fig. 3B).. To prevent the air tube from winding around the tendon wheel as a result of rotating with the tendon wheel once the RPC is activated, we limit the the maximum clutch range of RPC to 180 degrees (corresponding to 62.8 mm tendon stroke). Since most of the parts are 3D

printed (PLA), the RPC is lightweight (75 g) and low-cost.

We connected six RPCs in parallel to accomplish a one-to-more transmission (see Fig. 4). All drive wheels are connected in series to the motor by a coupling. All RPCs' airbags are activated with the same pneumatic pressure but at independent timings by six switching valves. This allows the RPCs to independently transmit force to each tendon which remotely actuates the corresponding finger via a Bowden tube. The whole actuation system including the geared motor and all RPCs is 903 g weight (150.5 g per DoF), 25 cm long, 6 cm wide, and 6 cm high.

D. Portable Circuit System

A portable circuit system is crucial for the robotic humanoid hand. The geared motor in the one-to-more transmission is controlled by a DC motor controller (20A-19S, JINSHENG). As it is challenging to integrate the pneumatic drive system into a compact robotic hand due to limited space, we use an off-board pneumatic drive system which includes the compressed air source and the pressure regulator. To pressurize the airbags in the RPCs, compressed air is stored in a portable capsule (RideAir, RIDEAIR), and the air pressure is controlled by a pressure regulator (ITV0031-2US, SMC). A series of solenoid valves (S070M-SCG-40, SMC) are used to switch RPCs on/off. A microcontroller (Arduino Uno) controls the pressure regulator and valves and can communicate with the PC. The motor and pneumatic electronic components of the SMUFR hand are driven by a 2600 mAh lithium battery.

To show its potential to fit in the anthropomorphic dimensions for a humanoid robot, we integrated all the components on a compact wearable vest (see Fig. 5). The entire actuation system including the battery and the gas cylinder weighs 2.77 kg, with dimensions of 32 cm length, 15 cm width and 5.5 cm height. Integrating our portable circuit system into a real humanoid robot is feasible by mounting it on the robot's back. Our portable circuit system enables humanoid robotic arms to manipulate our SMUFR hand in a large space, which stretches its application prospects.

III. MODELING

The load capacity of the RPC is correlated with the pneumatic pressure inside the airbag. Here, we build a mathematical model to calculate the maximum friction between the clutch plate and the drive wheel as follows,

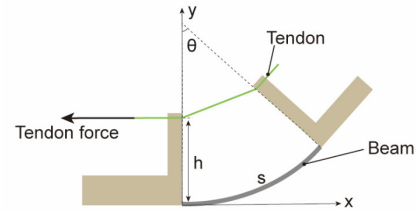


Fig. 6. The bending beam-based compliant joint.

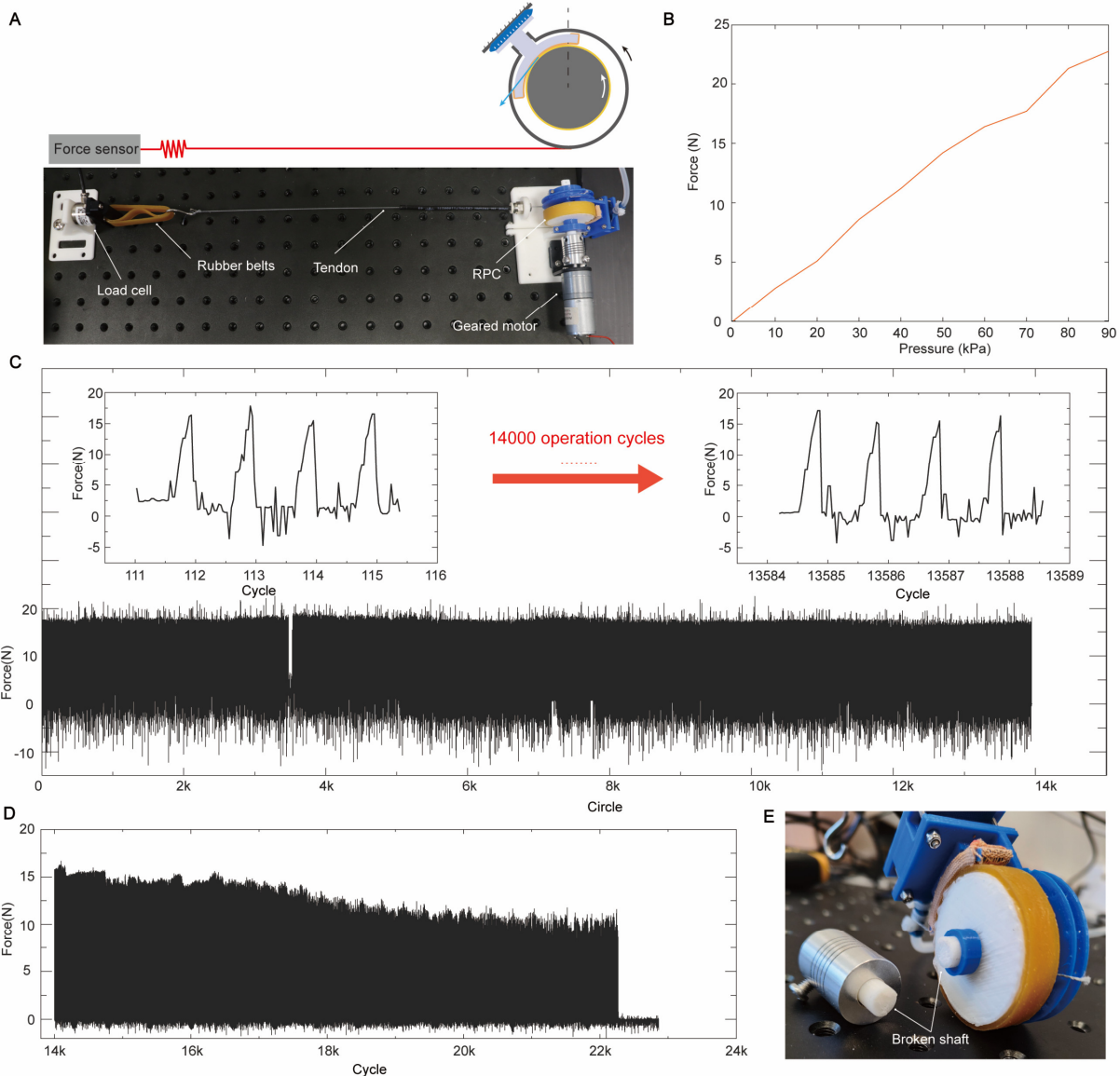


Fig. 7. Load Capacity and Durability of RPC. (A) The testing setup. (B) The maximum output force of RPC. (C) The durability test of RPC. (D) The output force after 14000cycles. (E) The broken shaft of RPC.

$$F_t = \frac{d_{DW}}{d_{TW}} \mu P S , \quad (1)$$

where F_t is the maximum transmitted force to the tendon, d_{DW} (40 mm) and d_{TW} (40 mm) are the diameters of the drive wheel and tendon wheel, P is the pneumatic pressure, S is the contacting area between the airbag and clutch plate, and μ is the friction coefficient between the friction strip and rubber band.

A feasible mathematic model for the finger with our beam-based compliant joints is also needed to calculate the tendon force and the bending angle of compliant joints. Since the bending degree is large, the theoretical model is demonstrated as the following equation,

$$\frac{\frac{d^2 y}{dx^2}}{[1 + (\frac{dy}{dx})^2]^{\frac{3}{2}}} = \frac{M(x)}{EI} , \quad (2)$$

$$I = \frac{bt^3}{12} , \quad (3)$$

where E is Young's modulus of the 301 stainless steel beam which is about 190 GPa, I is the Area Moment of Inertia for the beam, b is the width of the beam (15 mm), t is the thickness of the beam (0.2 mm), x and y are the positions of the beam, and $M(x)$ is the moment at x . (2) accurately described the bending deformation of the beam. However, this is a second-order nonlinear differential equation which is challenging to solve. To simplify the calculation, we assume the curvature of bending deformation is constant (see Fig. 6) as also seen in other literature [33], [34]. Thus, we have the

geometric equation,

$$x^2 + (y - \frac{s}{\theta})^2 = (\frac{s}{\theta})^2, \quad (4)$$

where s is the length of the beam (MCP: 22.2 mm, DIP & PIP: 16.5 mm) and θ is the central angle (bending angle). We insert (4) to (2) to get the mechanics equation,

$$\frac{\theta}{s} = \frac{M(x)}{EI}. \quad (5)$$

According to (5), the bending moment $M(x)$ is irrelevant with x and can be calculated directly given a bending angle θ . However, $M(x)$ can also be calculated by the tendon force F and is relevant with x ,

$$M(x) = F \cos(\frac{\theta}{2}) [x \tan(\frac{\theta}{2}) + h - y]. \quad (6)$$

where h is the distance between the tendon hole to the beam (11 mm). To minimize this contradiction, we firstly calculate the constant moment $M(x)$ by (5) at a given bending angle θ . Second, we use this constant moment to calculate the different pulling forces F along the beam. We divide the beam into 20 segments along the x direction (from 0 to $s \times \sin(\theta/\theta)$) and feed the sequence to x to calculate 20 different pulling forces F according to (6). Third, we average the 20 forces as the sole theoretical tendon force. By giving the bending angle from 1 to 90 degrees, we can calculate the corresponding theoretical tendon force. Thus, we can find the numerical relationship between the theoretical tendon force and the bending angle of the compliant joint.

We can extend this model to all compliant joints of a finger, and then obtain the relation between the tendon force and the pulling distance of the tendon. The pulling distance D_i can be calculated as follows,

$$D_i = \sum_{i=1}^3 [s_i - 2 \sin(\frac{\theta_i}{2}) (\frac{s_i}{\theta_i} - h)], \quad (7)$$

where i is the joint number (1: MCP, 2: PIP, 3: DIP).

IV. EXPERIMENTS AND RESULTS

A. Load Capacity and Durability of RPC

Based on the principle of RPC, the maximum output force of the RPC is related to the pneumatic pressure. The mathematical model as shown in (1) also indicates other parameters that can influence the output force. However, they are determined by design. Only the pneumatic pressure is controllable, hence, we tested the maximum output force of RPC under different pneumatic pressures.

We connected the tendon to a force gauge (HP-10, HANDPI) via a spring (see Fig. 7A). The spring was used to buffer the peak force which was recorded by the force gauge. First the DC geared motor is powered to spin the drive wheel at a constant speed (5 r/min). Then, we controlled the pneumatic pressure inside of the airbag to a target value and recorded the maximum tendon force recorded by the force gauge. We tested the maximum pulling force under different pneumatic pressures from 0 kPa to 90 kPa with a 10 kPa increment. The results shown in Fig. 7B indicate that the maximum output force increases proportionally with the pneumatic pressure

which fits the trend shown in the mathematic model. The maximum output force of RPC is approximately 23 N under 90 kPa pressure.

As the pneumatic clutches use frictional force (tangential) between the friction strip and the drive wheel, durability testing is also needed for our RPC. The output force of RPC determines the power of grasping objects. Thus, we tested the durability in terms of output force. The experiment setup was the same as the load capacity test in Fig. 7A. We periodically activated the RPC for 0.8 s and deactivated the RPC for 1.5 s and recorded the output force (see Fig. 7C). The pressure was set to a constant value of 80 kPa. The testing results show that the RPC can maintain the output force (constant peak force: 15 N) within 17000 cycles of activation and deactivation. Between the 17,000th and 22,000th cycle, the peak force decreased gradually to 11 N, as shown in Figure 7D. Subsequently, the force dropped to 0 N around the 22,000th cycle. This decrease occurred because the 3D-printed PLA shaft of the RPC experienced fatigue and ultimately broke, as depicted in Figure 7E.

B. The Tendon Force and Bending Angle

The movement of the robotic humanoid hand is actuated by the tendon force. Here, we tested the actual bending angle of the index finger's compliant joints (DIP, PIP, and MCP joints) and the tendon force. The finger's metacarpal phalanx is fixed. We connected the tendon to a force gauge, and mount the force gauge to a movable platform which is driven by a ball screw and a stepper motor (see Fig. 8A). Then, we controlled the platform to move by constant 4 mm increment and pull the tendon. The force gauge measured the tendon force. Meanwhile, the movement of the finger was recorded by a camera. In addition, we measured the bending angles θ of the three compliant joints by post-processing the video (Tracker 6.1.1).

The experimental results are shown in Fig. 8B. As tendon force increases, the bending angles of all three joints increases. The DCP joint has the least bending angle which is only about 0.6 rad at a 15 N tendon force, while the bending angle increment of the MCP joint is bigger than others with the same tendon force increment. Compared with the mathematic model (mentioned in section III), the experimental result of the MCP joint almost follows the model's trend where the growth rate of the bending angle slows down with increasing tendon force. For the PIP joint, its bending angle only fits the model well from 0 N to 5 N tendon force. Beyond 5 N, the actual bending angle is less than its theoretical value. The deviation between the DIP joint's bending angle and its model is the greatest, and the deviation increases with the tendon force. The growth rate of the PIP and DIP tendon forces decreases with increasing bending angle, since a higher bending angle generates higher friction on the tendon and declines the actual tendon force for PIP and DIP joints.

Furthermore, we demonstrate the relationship between the actual tendon force and the pulling distance of the tendon (see Fig. 8C). The tendon force grows with the pulling displacement and fits the mathematical model well. The maximum tendon force is less than 16 N which is within the load capacity of our RPC.

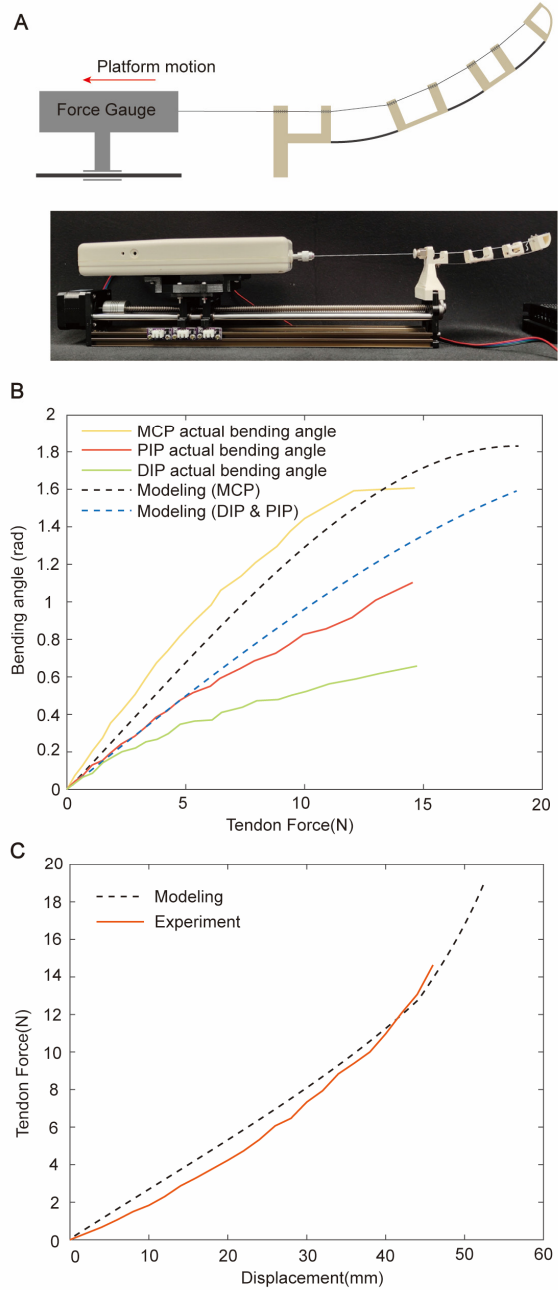


Fig. 8. Tendon force and bending angle testing. (A) The testing setup. (B) The bending angles of compliant joints with the tendon force. (C) The tendon forces with the pulling distance of tendon.

C. Dexterity and Adaptability of SMUFR Hand

Although the robotic hand is driven by a single motor, its dexterity is possible due to our one-to-more transmission system. We verified the dexterity and grasping functions through experiments. By activating the RPC of the thumb only, the thumb flexed as expected (see Fig. 9A and Video S2). We then activated RPCs for other fingers, which also caused them to bend correspondingly. We can also achieve two fingers flexion simultaneously in a similar way (see Fig. 9B and Video S2) as well as four fingers flexion. In contrast with other tendon-driven dexterous robotic hands with many driving motors

[35]–[38], SMUFR hand has only 6 actuated DoFs which limits its operating dexterity. However, considering the single driving motor, our robotic hand demonstrated relatively high dexterity.

To verify its grasping functions, we selected unique objects of different sizes and shapes, including a USB flash driver (10 g), a ping-pong ball (3 g), an IC card (5 g), a magic cube (76 g), an apple (189 g), two bananas (374 g), a coffee mug (310 g), a hammer (358 g), a bottle of water (1 kg) and a carton box (190 g). The robotic hand is able to grab these items via different gestures (see Fig. 9C and Video S3). Furthermore, our SMUFR hand can move and grasp in an underwater environment (see Video S4) since there are no electronic components in the robotic hand. This ability could empower the wearer to do more daily activities like washing fruits and vegetables in the kitchen.

D. Holding Force and Fingertip Force of SMUFR Hand

The holding force of fingers is significant for the robotic hand to manipulate heavy items. Hence, we tested the holding force of a single finger. Firstly, we fixed the hand vertically and put a bar over the palm (see Fig. 10A). The bar was also connected to a force gauge that was mounted on a movable tensile machine (JSV H1000, MEASURING INSTRUMENT TECH). Secondly, the geared motor and the RPC are activated, with different pneumatic input pressures (15, 30, 50, 90, and 120 kPa) being applied into the airbag of the RPC, which results in the finger hooking over the bar (see Fig. 10A). Lastly, the tensile machine to pull the bar out of the palm at a constant velocity (100 mm/min). The force resisting the bar from the finger (the holding force) was measured by the force gauge. The experimental holding force with the pulling displacement under different pneumatic pressure in the airbag is shown in Fig. 10A. When the bar is pulled up, the holding force increases with the displacement, and then drops down to 0 sharply when the bar escaped the finger's wrap. From 15 kPa to 90 kPa, the maximum holding force (peak value) increases with the pneumatic pressure and is about 17 N under 90 kPa. However, the peak holding force almost remains constant when the pneumatic pressure passes 90 kPa.

Additionally, we also tested the fingertip force at two finger configurations: straight state (see Fig. 10B) and closed state (see Fig. 10C). The fingertip force capacity at straight state can indicate SMUFR hand's distal output force. With the finger in a straight and horizontal configuration, a force gauge is placed vertically on the fingertip to measure the contact force with the fingertip when the RPC for that particular finger is activated. The testing results (see Fig. 10B) illustrate that the fingertip force in this straight configuration is low (about 1.5 N). This is because the beams of the finger bend outwards as the tendon pulls. The stiffness of beam is too low to provide a high fingertip force at this configuration. The fingertip force was then tested with the finger in a closed configuration and a load cell mounted on the base (palm) of the finger (see Fig. 10C) to reflect the grasping power of the finger. The fingertip force in this closed configuration is much higher (up to 11 N with 120 kPa pressure applied to the RPC, see Fig. 10C). The fingertip force increases with increasing applied pneumatic pressure to the RPC.

Subsequently, we demonstrated our SMUFR hand grasping a 4 kg dumbbell, while being vertically lifted up (see Fig. 10D)

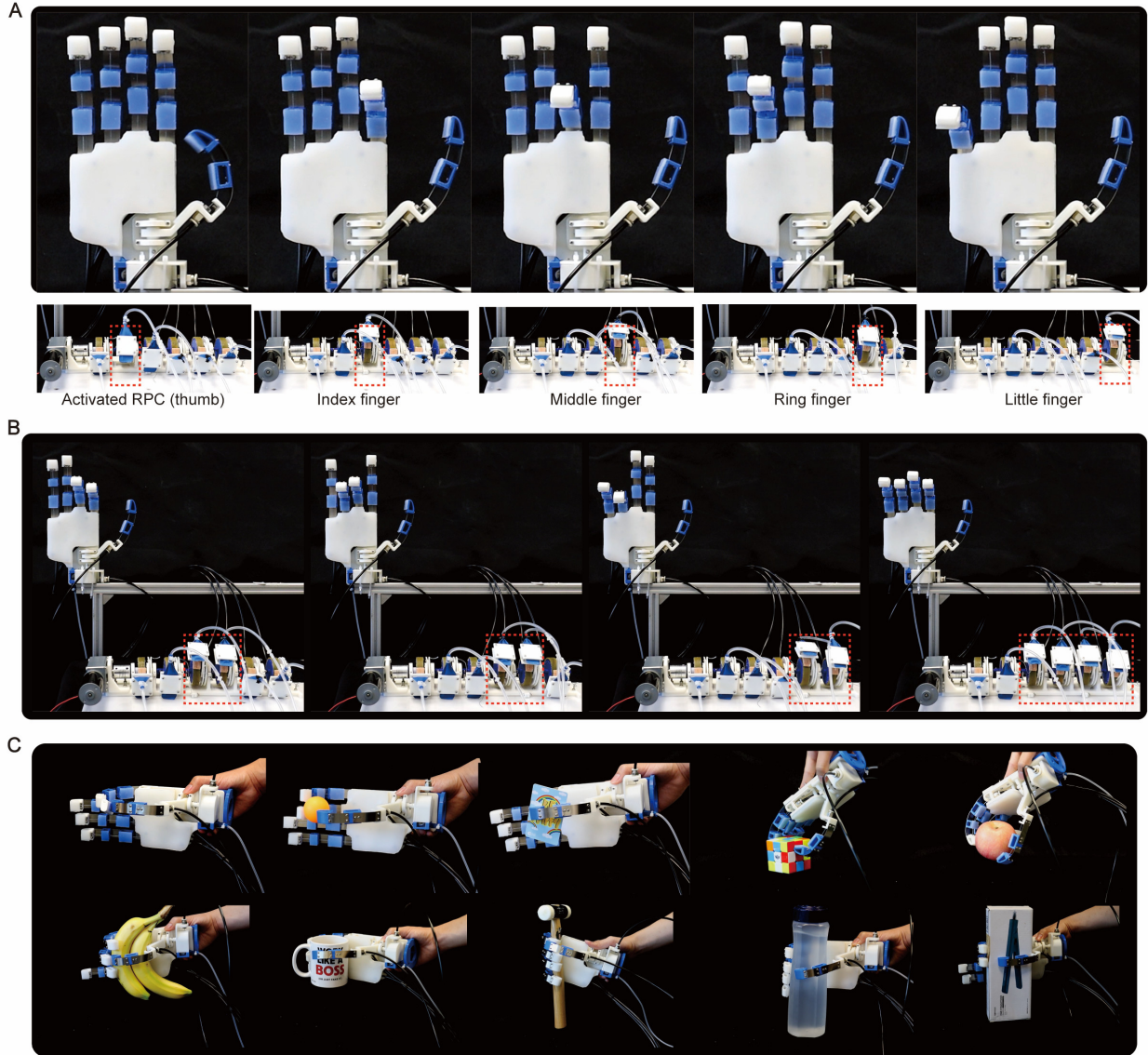


Fig. 9. The dexterity and grasping functions of SMUFR hand. (A) A single finger flexion. (B) Multiple fingers flexion. (C) SMUFR hand can grasp objects with different sizes, shapes and weights.

and Video S5) to display its high holding force. The SMUFR hand was also used to grasp a 4.2 kg dumbbell at different orientations (see Fig. 10E and Video S5). We further evaluated the hand's performance by testing its ability to grasp a load in the lateral direction, as illustrated in Fig. 10F and Video S5. In this particular grasping setup, the load capacity was found to be diminished to 2.3 kg due to the finger's high compliance and its limited resistance to shear force.

E. High Robustness and Compliance of SMUFR Hand

To demonstrate the robustness of our robotic finger design, we tested its bending durability by pulling the tendon repeatedly (see Video S6). A linear ball-screw tensile machine was used to pull the tendon and the tensile stroke was set to 5 cm to fully close the finger (see Fig. 11A). After fully closed, the finger can return to its initial position. We took photos of the finger at its initial positions after 0, 100, 1k, 2k, 3k, 5k, 8k, 10k, 14k, 20k and 30k cycles, and measured the bending angle

(the angle between the distal phalanx and the metacarpal phalanx) of the finger by using Tracker software. The results shown in Fig. 11A indicated that the bending angle variation of the robotic finger was 6.5 degree after 30000 fully closed cycles (11.7 degree of 0 cycle and 18.2 degree of 30000 cycles), and remained almost constant after 15000 cycles. By conducting the durability test illustrated in Fig. 11A, we confirmed the robustness and safety of the stainless beam. It demonstrated satisfactory durability by withstanding 30000 closing and opening cycles without any breakage. While the 6.5-degree deviation impacts the graspable aperture, the total bending angle of the finger, at 18.2 degrees, might still be deemed acceptable. This angle represents only half of the typical human finger's bending angle, which is approximately 35 degrees, during its resting state [39]. However, this deviation can be rectified simply by bending the finger in the opposite direction.

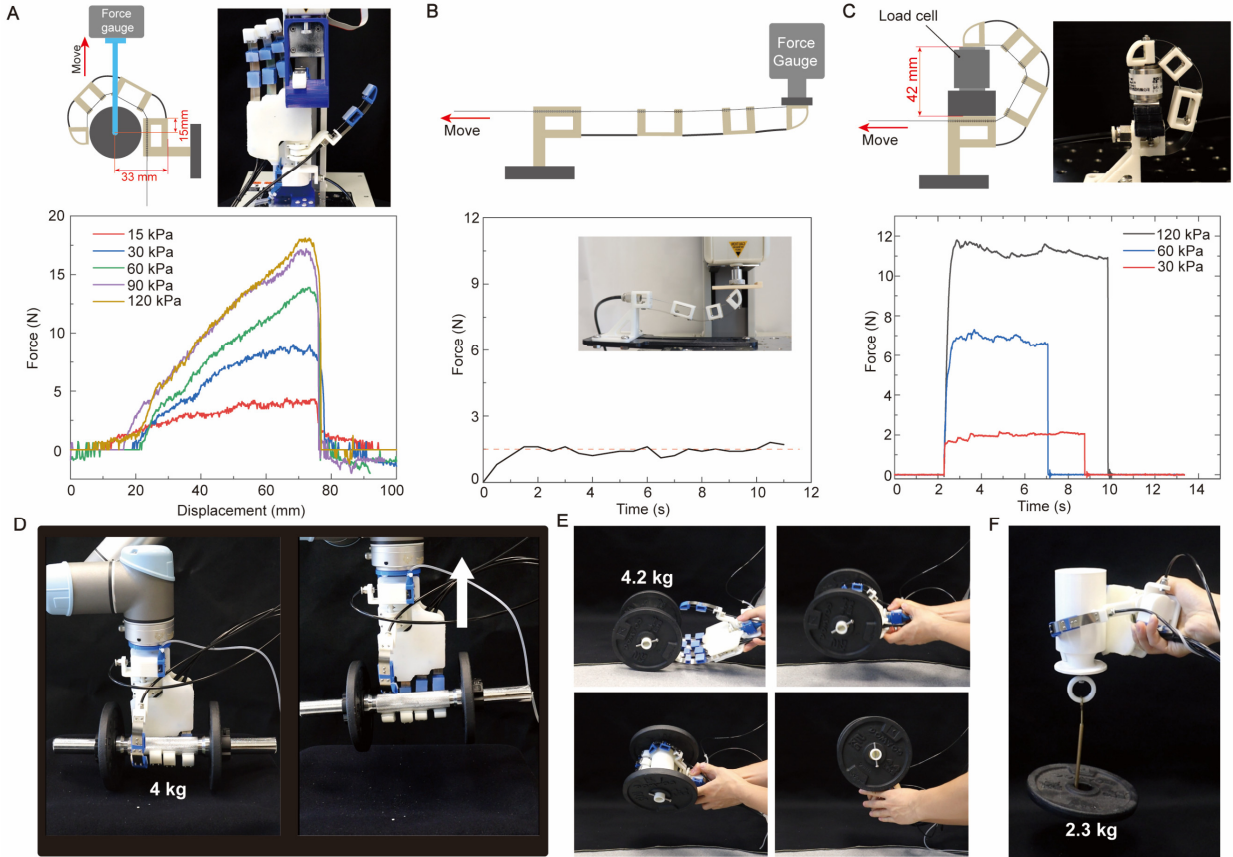


Fig. 10. The comprehensive force test for SMUFR hand. (A) The testing setup and results of finger holding force. (B) The testing setup and results of fingertip force at straight configuration. (C) The testing setup and results of fingertip force at closing configuration. (D) The SMUFR hand can lift and hold a 4 kg dumbbell. (E) The SMUFR hand can grasp a 4.2 kg weight at multiple orientations. (F) The SMUFR hand can laterally grasp a 2.3 kg weight.

Our robotic hand possesses high bidirectional bending compliance, which makes it very safe during interaction with a human. The robotic finger can bend adaptively when subjected to the low contacting force applied by a human fingertip (see Fig. 11B). After the interaction, it can also restore itself to the straight configuration due to the elastic nature of the finger joint. In addition, fingers of the SMUFR hand display outstanding twisting compliance. The robotic finger can twist adaptively when subjected to twisting torque (see Video S6 and Fig. 11B) and return to its initial position after releasing the torque.

The resistance to shear force applied to the beam was also investigated by experiments. We applied a 10 N shear force to the beams of finger by hanging a 1 kg weight to the intermediate and proximal phalanxes respectively, and we picked up the finger. The beam of MCP joint can fully resist the 10 N shear force applied to proximal phalanx but significantly deformed while the shear force was applied to intermediate phalanx (see Video S6 and Fig. 11C). Meanwhile, the beam of PIP joint remained planar. This is because the shear torque applied to the beam of MCP joint increased twice due to the increased perpendicular distance from the applied shear force.

V. CONCLUSION

In this paper, the authors present a robotic humanoid hand (SMUFR hand) with high bidirectional compliance and dexterity, and a compact and lightweight one-to-more transmission. By designing a flexible beam-based bending joint, our robotic humanoid hand is very compliant, allowing for safe interaction with the environment and human. A compact thumb rotation joint with a pneumatic locking mechanism was deployed into our SMUFR hand, which improved its grasping adaptability and performance. Moreover, we developed a lightweight and low-cost rotary pneumatic clutch capable of outputting a 23 N force, and based on it, the one-to-more actuation system which can split the single motor's power to five fingers independently was also accomplished. We also developed a mathematical model to predict the actual tendon force and joint bending angle. The experimental results of the bending angle approximately follow the trend of the mathematical model, and the experimental tendon force result fits the model well. We then displayed the dexterity and grasping functions of the SMUFR hand through different gestures. It is worth mentioning that our SMUFR hand can achieve underwater grasping due to its non-electronic hand. A characterization test was conducted to demonstrate its high holding force (up to 17 N for one finger)

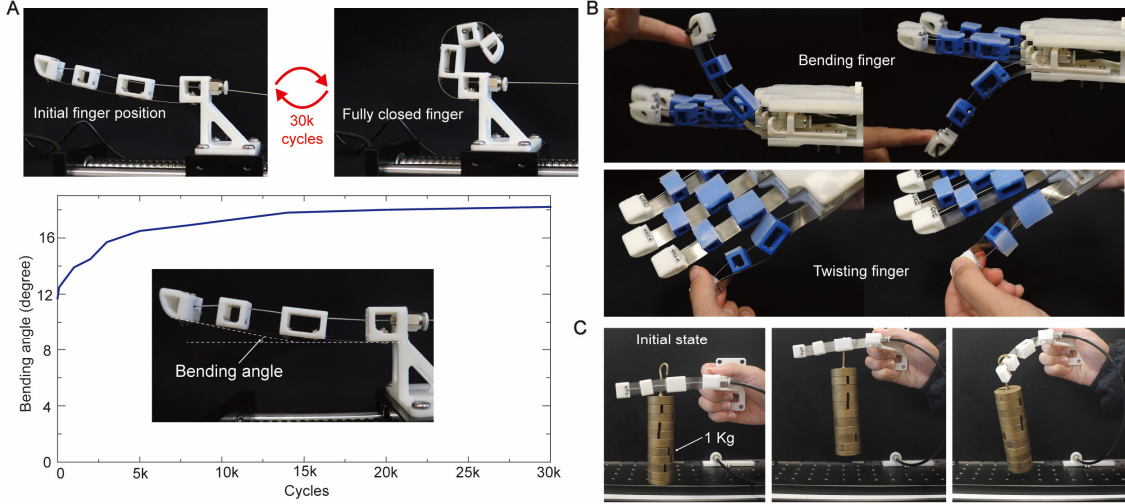


Fig. 11. The robustness and compliance test of SMUFR hand. (A) The durability test of the robotic finger. (B) The bending and twisting compliance of the finger. (C) The resistance to shear torque applied to the beams of the finger.

capable of grasping even a 4 kg dumbbell. Our SMUFR humanoid hand and its one-to-more actuation system can also be integrated into a full-body humanoid robot to achieve a safe and dexterous humanoid robot.

In contrast with other robotic humanoid hands [17], [36], [37], [40]–[44], our SMUFR hand has only one driving motor and a pneumatic pressure regulator, which implies its lower cost. Moreover, our robotic hand is lightweight (0.36 kg), but can grasp and hold a 4 kg payload (see TABLE I). Our SMUFR hand possesses 6 active DoFs that is on par with other robotic hands, and has sufficient dexterity in terms of hand manipulation for daily living. Furthermore, our robotic hand has higher unidirectional bending and twisting compliance, resulting from its ultraflexible joint design. However, the fingertip output force in its straight finger state is only 1.5 N, which may restrict the usage of our robotic hand in certain use cases such as pressing a button. The fingertip force in its closed finger state is 12 N which shows its strong grasping power. Besides limited use case in the straight

configuration of the finger, there are some other limitations in this work. The friction between the tendon and the phalanx hole increases when the joint bends at a large angle, which reduces the tendon force of the distal joints (especially PIP and DIP joints). This may attribute to the significant deviation of the bending angles of these two joints from the mathematical model when the joints bend at a large angle.

In the future, we will optimize the phalanx architecture to reduce friction during joint bending and design some soft and elastic skin for the robotic hand to increase its grasping ability and its cosmetic appearance. The specific human-robot interaction applications for our humanoid robotic hand will be explored in the next stage. We may also deploy more RPCs to achieve more DoF actuation. On the other hand, we are able to amplify the output force for higher force requirement, by connecting multiple RPCs output tendons in parallel. Last, we will use metal materials such as aluminum to fabricate the RPC for higher durability.

TABLE I
COMPARISON WITH OTHER ROBOTIC HUMANOID HAND

Ref	[43]	[44]	[41]	[40]	[36]	[42]	[17]	[37]	This work
Actuation method	Geared motors + rigid link		Tendon	Tendon	Tendon	Tendon + rigid link	Tendon	Tendon + rigid link	Tendon
Number of motors (pneumatic pressure regulators)	4	16	2	6	15	15	5	3	1+1*
Max Payload (kg)	-	1.5	-	-	0.9	1.8	0.9	-	4
Active DoFs (DoAs)	4	16	2	6	15	15	5	3	6
Compliance**	Low	Low	Medium	Medium	Medium	Low	Medium	Low	High
Fingertip output force (N)	31.4	4	11.73	-	6	3	-	10	1.5/12 ***
Weight (kg)	0.478	0.9	0.38	0.35	0.9	0.8	0.546	0.88	0.36

* One driving motor and one pneumatic pressure regulator.

** Low: the finger cannot deform subjected to external force with stopped motor; Medium: one-way bending compliance or part of joints compliance;

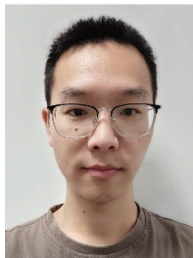
High: unidirectional bending compliance.

*** 1.5 N at straight finger state; 12 N at closed finger state.

REFERENCES

- [1] S. Kajita, H. Hirukawa, K. Harada, and K. Yokoi, *Introduction to humanoid robotics*, vol. 101. Springer, 2014.
- [2] Y. Tong, H. Liu, and Z. Zhang, “Advancements in Humanoid Robots: A Comprehensive Review and Future Prospects,” *IEEE/CAA J. Autom. Sin.*, vol. 11, no. 2, pp. 301–328, 2024.
- [3] K. S. Welfare, M. R. Hallowell, J. A. Shah, and L. D. Riek, “Consider the human work experience when integrating robotics in the workplace,” in *2019 14th ACM/IEEE international conference on human-robot interaction (HRI)*, IEEE, 2019, pp. 75–84.
- [4] D. M. West, *The future of work: Robots, AI, and automation*. Brookings Institution Press, 2018.
- [5] G. Gioioso, G. Salvietti, M. Malvezzi, and D. Prattichizzo, “Mapping synergies from human to robotic hands with dissimilar kinematics: an approach in the object domain,” *IEEE Trans. Robot.*, vol. 29, no. 4, pp. 825–837, 2013.
- [6] Y. Li *et al.*, “A dual-mode actuator for soft robotic hand,” *IEEE Robot. Autom. Lett.*, vol. 6, no. 2, pp. 1144–1151, 2021.
- [7] B.-Y. Sun *et al.*, “Design principle of a dual-actuated robotic hand with anthropomorphic self-adaptive grasping and dexterous manipulation abilities,” *IEEE Trans. Robot.*, vol. 38, no. 4, pp. 2322–2340, 2021.
- [8] Y. Kim, T. Jang, H. Gurung, N. A. Mansour, B. Ryu, and B. Shin, “Bidirectional rotating actuators using shape memory alloy wires,” *Sensors Actuators A Phys.*, vol. 295, pp. 512–522, 2019.
- [9] F. Negrello, H. S. Stuart, and M. G. Catalano, “Hands in the real world,” *Front. Robot. AI*, vol. 6, p. 147, 2020.
- [10] J. Ueda, M. Kondo, and T. Ogasawara, “The multifingered NAIST hand system for robot in-hand manipulation,” *Mech. Mach. Theory*, vol. 45, no. 2, pp. 224–238, 2010.
- [11] S. R. Kashef, S. Amini, and A. Akbarzadeh, “Robotic hand: A review on linkage-driven finger mechanisms of prosthetic hands and evaluation of the performance criteria,” *Mech. Mach. Theory*, vol. 145, p. 103677, 2020.
- [12] Y. Wang, W. Li, S. Togo, H. Yokoi, and Y. Jiang, “Survey on main drive methods used in humanoid robotic upper limbs,” *Cyborg Bionic Syst.*, 2021.
- [13] R. Deimel and O. Brock, “A novel type of compliant and underactuated robotic hand for dexterous grasping,” *Int. J. Rob. Res.*, vol. 35, no. 1–3, pp. 161–185, 2016.
- [14] Q. Xiong, X. Zhou, J. W. Ambrose, and R. C.-H. Yeow, “An Amphibious Fully-Soft Centimeter-Scale Miniature Crawling Robot Powered by Electrohydraulic Fluid Kinetic Energy,” *Adv. Sci.*, vol. 2308033, pp. 1–14, 2023, doi: 10.1002/advs.202308033.
- [15] T. Hao, H. Xiao, S. Liu, C. Zhang, and H. Ma, “Multijointed pneumatic soft hand with flexible thenar,” *Soft Robot.*, vol. 9, no. 4, pp. 745–753, 2022.
- [16] P. M. Khin, J. H. Low, M. H. Ang Jr, and C. H. Yeow, “Development and grasp stability estimation of sensorized soft robotic hand,” *Front. Robot. AI*, vol. 8, p. 619390, 2021.
- [17] L. Liow, A. B. Clark, and N. Rojas, “Olympic: A modular, tendon-driven prosthetic hand with novel finger and wrist coupling mechanisms,” *IEEE Robot. Autom. Lett.*, vol. 5, no. 2, pp. 299–306, 2019.
- [18] A. McLaren, Z. Fitzgerald, G. Gao, and M. Liarokapis, “A passive closing, tendon driven, adaptive robot hand for ultra-fast, aerial grasping and perching,” in *2019 IEEE/RSJ International Conference on Intelligent Robots and Systems (IROS)*, IEEE, 2019, pp. 5602–5607.
- [19] J. K. Paik, B. H. Shin, Y. Bang, and Y.-B. Shim, “Development of an anthropomorphic robotic arm and hand for interactive humanoids,” *J. Bionic Eng.*, vol. 9, no. 2, pp. 133–142, 2012.
- [20] Z. Lu, H. Guo, W. Zhang, and H. Yu, “GTac-Gripper: A Reconfigurable Under-Actuated Four-Fingered Robotic Gripper With Tactile Sensing,” *IEEE Robot. Autom. Lett.*, vol. 7, no. 3, pp. 7232–7239, 2022.
- [21] H. Yang *et al.*, “A low-cost linkage-spring-tendon-integrated compliant anthropomorphic robotic hand: MCR-Hand III,” *Mech. Mach. Theory*, vol. 158, p. 104210, 2021.
- [22] W. Ryu, Y. Choi, Y. J. Choi, Y. G. Lee, and S. Lee, “Development of an anthropomorphic prosthetic hand with underactuated mechanism,” *Appl. Sci.*, vol. 10, no. 12, p. 4384, 2020.
- [23] D. Wei *et al.*, “Electrostatic Adhesion Clutch with Superhigh Force Density Achieved by MXene-Poly(Vinylidene Fluoride–Trifluoroethylene–Chlorotrifluoroethylene) Composites,” *Soft Robot.*, Nov. 2022, doi: 10.1089/soro.2022.0013.
- [24] M. Xiloyannis *et al.*, “Design and validation of a modular one-to-many actuator for a soft wearable exosuit,” *Front. Neurorobot.*, vol. 13, p. 39, 2019.
- [25] M. Canesi, M. Xiloyannis, A. Ajoudani, A. Bicchi, and L. Masia, “Modular one-to-many clutchable actuator for a soft elbow exosuit,” in *2017 International Conference on Rehabilitation Robotics (ICORR)*, IEEE, 2017, pp. 1679–1685.
- [26] E. J. Rouse, L. M. Mooney, and H. M. Herr, “Clutchable series-elastic actuator: Implications for prosthetic knee design,” *Int. J. Rob. Res.*, vol. 33, no. 13, pp. 1611–1625, 2014.
- [27] H. Böse, T. Gerlach, and J. Ehrlich, “Magnetochemical torque transmission devices with permanent magnets,” in *Journal of Physics: Conference Series*, IOP Publishing, 2013, p. 12050.
- [28] D. M. Wang, Y. F. Hou, and Z. Z. Tian, “A novel high-torque magnetorheological brake with a water cooling method for heat dissipation,” *Smart Mater. Struct.*, vol. 22, no. 2, p. 25019, 2013.
- [29] S. Diller, C. Majidi, and S. H. Collins, “A lightweight, low-power electroadhesive clutch and spring for exoskeleton actuation,” *2016 IEEE Int. Conf. Robot. Autom.*, pp. 682–689, 2016, doi: 10.1109/ICRA.2016.7487194.
- [30] H. Kawasaki and T. Mouri, “Humanoid robot hand and its applied research,” *J. Robot. Mechatronics*, vol. 31, no. 1, pp. 16–26, 2019.
- [31] U. Kim *et al.*, “Integrated linkage-driven dexterous anthropomorphic robotic hand,” *Nat. Commun.*, vol. 12, no. 1, pp. 1–13, 2021.
- [32] L. Tian, J. Liu, N. M. Thalmann, D. Thalmann, and J. Zheng, “Design of a flexible articulated robotic hand for a humanoid robot,” in *2019 IEEE-RAS 19th International Conference on Humanoid Robots (Humanoids)*, IEEE, 2019, pp. 572–577.
- [33] W. Chen, C. Xiong, C. Liu, P. Li, and Y. Chen, “Fabrication and dynamic modeling of bidirectional bending soft actuator integrated with optical waveguide curvature sensor,” *Soft Robot.*, vol. 6, no. 4, pp. 495–506, 2019.
- [34] Q. Zhang, P. Yan, and H. Wang, “A curved-beam based quasi-constant force mechanism supporting large range and force-sensitive robotic manipulation,” *Mech. Mach. Theory*, vol. 172, p. 104799, 2022.
- [35] V. Kumar, Z. Xu, and E. Todorov, “Fast, strong and compliant pneumatic actuation for dexterous tendon-driven hands,” in *2013 IEEE international conference on robotics and automation*, IEEE, 2013, pp. 1512–1519.

- [36] S. Min and S. Yi, "Development of cable-driven anthropomorphic robot hand," *IEEE Robot. Autom. Lett.*, vol. 6, no. 2, pp. 1176–1183, 2021.
- [37] J. Kashiwakura, P. G. S. Alva, I. M. Guerra, C. Bona, S. F. Atashzar, and D. Farina, "Task-oriented design of a multi-degree of freedom upper limb prosthesis with integrated myocontrol and sensory feedback," *IEEE Trans. Med. Robot. Bionics*, 2023.
- [38] B. Fang, F. Sun, Y. Chen, C. Zhu, Z. Xia, and Y. Yang, "A tendon-driven dexterous hand design with tactile sensor array for grasping and manipulation," in *2019 IEEE International Conference on Robotics and Biomimetics (ROBIO)*, IEEE, 2019, pp. 203–210.
- [39] R. J. Schwarz and C. Taylor, "The anatomy and mechanics of the human hand," *Artif. Limbs*, vol. 2, no. 2, pp. 22–35, 1955.
- [40] J. Fajardo, V. Ferman, D. Cardona, G. Maldonado, A. Lemus, and E. Rohmer, "Galileo hand: An anthropomorphic hand and affordable upper-limb prosthesis," *IEEE access*, vol. 8, pp. 81365–81377, 2020.
- [41] P. Weiner, J. Starke, S. Rader, F. Hundhausen, and T. Asfour, "Designing prosthetic hands with embodied intelligence: the kit prosthetic hands," *Front. Neurorobot.*, vol. 16, p. 815716, 2022.
- [42] H. Yang *et al.*, "An affordable linkage-and-tendon hybrid-driven anthropomorphic robotic hand—MCR-Hand II," *J. Mech. Robot.*, vol. 13, no. 2, p. 24502, 2021.
- [43] M. Controzzi, F. Clemente, D. Barone, A. Ghionzoli, and C. Cipriani, "The SSSA-MyHand: a dexterous lightweight myoelectric hand prosthesis," *IEEE Trans. Neural Syst. Rehabil. Eng.*, vol. 25, no. 5, pp. 459–468, 2016.
- [44] D.-H. Lee, J.-H. Park, S.-W. Park, M.-H. Baeg, and J.-H. Bae, "KITECH-hand: A highly dexterous and modularized robotic hand," *IEEE/ASME Trans. Mechatronics*, vol. 22, no. 2, pp. 876–887, 2016.



Quan Xiong received the B.S. degree in mechanical design & manufacturing and their automation from Harbin Engineering University, Harbin, China, in 2018, and the M.S. degree in mechanical engineering from Harbin Institute of Technology, Harbin, China, in 2020. He was a research assistant in the Department of Mechanical and Energy Engineering at the Southern University of Science and Technology, Shenzhen, China, from 2020 to 2021. He is currently pursuing the Ph.D. degree in the Department of Biomedical Engineering, National University of Singapore, Singapore.

His research interests include novel actuator, soft robotics and medical robotics.



Dannuo Li received the bachelor's degree in biomedical engineering from Southwest Jiaotong University, Sichuan, China, in 2023. He is currently a master student at the EI lab, National University of Singapore, Singapore. His research interests include soft robotics, haptics, and human-robot interaction.



Zhou Xuanyi received the bachelor degree in Biomedical Engineering from Zhejiang University in 2023. Now he is the master student at EI Lab in College of Design and Engineering of National University of Singapore. His research interests include Pneumatic soft robots, HASEL actuators, underwater soft robots and applications for soft robots.



Wenci Xin received the B.Eng. degree in Mechanical Engineering from Huazhong University of Science and Technology, Wuhan, China, in 2019, and the M.Phil. degree in Surgery from the Chinese University of Hong Kong, Hong Kong, in 2021. He is currently working toward the Ph.D. degree in Mechanical Engineering with the Soft Robotics Lab in National University of Singapore, Singapore.

His research interests include biorobotics and soft robotics, especially in leveraging the potential of soft robots through bioinspired approaches.



Chao Wang received the M.S. degree in mechatronics engineering from the China University of Mining and Technology, China, in 2018, and received the Ph.D. degree in mechanical engineering from the Harbin Institute of Technology, China, in 2023. He is currently an assistant professor with the school of mechanical engineering, Nanjing University of Science and Technology. His research interests include object detection and robotic manipulation.



Jonathan Ambrose has a PhD specializing in soft artificial muscles and modular soft robots. He currently serves as a Research Fellow at the National University of Singapore, where his work focuses on wearable soft haptics and force feedback. Additionally, Jonathan is a co-founder of Seamless XR, a startup dedicated to developing hardware that enables touch interactions in VR/AR environments.



Raye Chen-Hua Yeow (Member, IEEE) received the Ph.D. degree in bioengineering from the National University of Singapore (NUS), Singapore, in 2010. He received postdoctoral training in biorobotics from Harvard University, Cambridge, MA, USA, from 2010 to 2012. He is an Associate Professor and Deputy Head (Outreach & Industry) with the Department of Biomedical Engineering and Advanced Robotics Center, NUS. He is the Program Lead for the Soft and Hybrid Robotics Program under the National Robotics Programme Office in Singapore. He is also currently a Visiting Professor with Computer Science and Artificial Intelligence Laboratory, Massachusetts Institute of Technology, Cambridge, MA, USA. He has authored or coauthored more than 180 journal and conference papers, more than research and innovation awards, and cofounded four soft robotics startups.